C. Wang, J. Wang, F. Campagnolo, D.B. Carraón, C.L. Bottasso
Validation of Large-Eddy Simulation of Scaled Waked Wind Turbines in Different Yaw Misalignment Conditions
Journal of Physics: Conference Series, Vol. 1037, N. 6, 2018, 062007 (11 pages)
doi:10.1088/1742-6596/1037/6/062007

Validation of large-eddy simulation of scaled waked wind turbines in different yaw misalignment conditions

IOP Conf. Series: Journal of Physics: Conf. Series **1037** (2018) 062007 doi:10.1088/1742-6596/1037/6/062007

Validation of large-eddy simulation of scaled waked wind turbines in different yaw misalignment conditions

C Wang[1], J Wang[1], F Campagnolo[1], D B Carreón[2] and C L Bottasso[1,3]

[1] Wind Energy Institute, Technische Universität München, Boltzmannstraße 15, D-85748 Garching bei München, Germany
[2] Instituto de Energías Renovables, Universidad Nacional Autónoma de México, Priv. Xochicalco s/n Temixco, Morelos 62580, Mexico
[3] Dipartimento di Scienze e Tecnologie Aerospaziali, Politecnico di Milano, Via La Masa 34, I-20156 Milano, Italy

E-mail: cy.wang@tum.de

Abstract.

This paper compares lifting-line large-eddy simulations (LES) of scaled wind turbines against experimental measurements obtained in a boundary layer wind tunnel. The final goal of this effort is to develop a verified digital copy of the experimental facility, in support of wind farm control research. Three scaled wind turbine models are arranged in different waked configurations and yaw misalignment conditions. In the experiments, the wind turbine response is measured in terms of various operational parameters, while the flow is measured with two scanning LiDARs. Simulation and experimental results are compared with respect to flow characteristics, turbine states and wake behavior. The analysis of the results shows a good match between simulations and experiments. Besides this important verification, the numerical simulations are also used to explain a wake interference phenomenon observed in the experiments, which causes a modification in the path of the wake of shaded turbines.

1. Introduction

Among existing wind farm control strategies, yaw-based control appears to be very promising in spite of its apparent simplicity [1]. Using this control approach, upstream wind turbines are yawed slightly out of the wind with the goal of steering their wakes away from downstream turbines. A wind farm super-controller is then tasked with the goal of finding the optimal yaw angles for each wind turbine, which optimize some performance index while satisfying desired operational constraints.

In support of wind plant control research, our group has developed scaled wind turbines [2] that can be operated in a boundary layer wind tunnel. The wind turbines are governed by their individual controllers, but are also optionally managed in a collective manner by a wind farm super-controller.

A first goal of the present paper is to compare the results of a LES model of the scaled test facility with experimental measurements at different constant-in-time yaw misalignment angles. Various operational conditions are considered, which correspond to different overlaps of the shed

wakes with the downstream wind turbines. The present static validation is an intermediate step towards the validation of the dynamic case, where the yaw angles change in time.

A second goal of the paper is to explain a wake interference effect observed in the experiments. Specifically, it appears that one of the downstream wake-shaded turbines exhibits a larger wake deflection than expected by its nominal misalignment angle with the free stream. Numerical simulations are used to show that this phenomenon can be qualitatively explained by the sidewash caused by the shading wake, which has the effect of modifying the flow direction at the downstream turbine rotor disk and of translating its wake path sideways.

2. Experimental setup

A cluster of three wind turbines is operated in the wind tunnel. The wind turbine rotors have a diameter of 1.1 m, and were designed to match the TSR and circulation distribution of a full-scale reference machine, resulting in a realistic wake behavior [2]. Spires are placed at the tunnel inlet and work as turbulence generators. Vortices shed by the spires result in quasi-isotropic turbulence where the wind turbine models are located. The longitudinal distance between each wind turbine is 4D, while the lateral distance is 0.5D. The static experiments are conducted at different yaw settings of the various machines. Figure 1 shows a top view of the wind tunnel when the wind turbines are optimally yawed for overall power capture, which corresponds to 20 deg and 16 deg of the first and second machine, respectively. The optimal yaw angles were determined experimentally. A more detailed description of the experiments is given in Refs. [2,3].

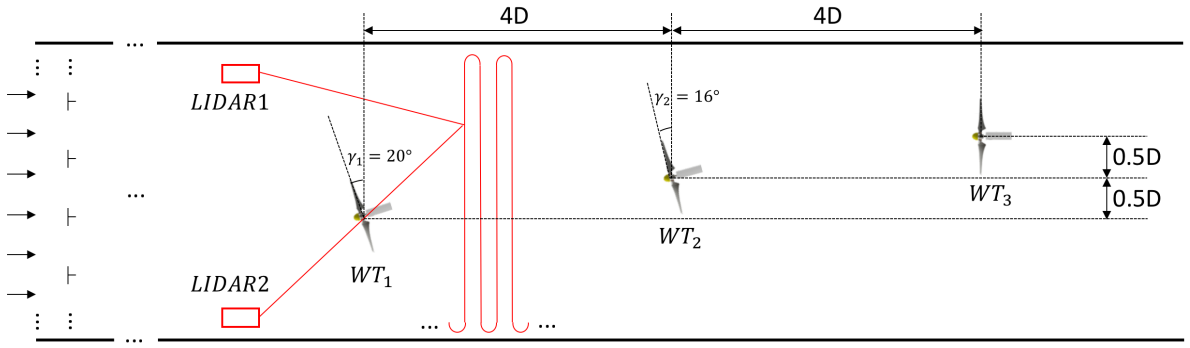

Figure 1: Top view of the wind tunnel experiment: from left to right, chamber inlet, turbulence generating spires, scanning LiDARs, upstream wind turbine WT1, example of LiDAR scanning path, downstream turbine WT2, and downstream turbine WT3.

One of the highlights of the experiment is the measurement of the flow with two scanning LiDARs [3]. The velocity field at a horizontal plane 0.09D above hub height is measured, neglecting the vertical velocity component. The red curve in Fig. 1 depicts the scanning path of the LiDARs, which takes 18.48 sec to be completed. An average flow field is obtained by averaging the LiDAR data over 30 passes [3].

3. Numerical model

The numerical simulation environment is based on the open-source code `Foam-extend-4.0`. The model is based on a finite-volume LES formulation, implemented in the code `SOWFA` [4], coupled with a lifting line model of the blades, whose implementation is based on `FAST v8` [5]. The turbine nacelle and tower are modelled by an immersed boundary method [6]. The airfoil polars are determined by a singular-value-decomposition-based system identification procedure [7]. By

this method, the aerodynamic characteristic of the airfoils are obtained using experimental measurements of the rotor thrust and torque at various operating points [2]. This same simulation environment has been previously compared to scaled experimental measurements in Refs. [8–10] in wind aligned conditions. The present paper extends that analysis to yaw misaligned conditions, which are relevant to the problem of wind farm control.

The simulation model includes the wind tunnel walls and the passive generation of turbulence obtained by the use of spires placed at the tunnel inlet. The simulation of the flow around the spires is particularly expensive, as it must faithfully represent the breakdown of the spire-shed vortices into a sheared and turbulent flow. In fact, a high-quality dense mesh —obtained by the mesh generator `ANSYS/ICEM`— is used to resolve the flow around the spires. Since the same turbulent flow can be used for several simulations characterized by different operating conditions of the wind turbines, the overall wind tunnel chamber is split into two separate computational domains. One models the tunnel inlet, the spires and the development of the turbulent flow, up to a distance of 36 m downstream of the inlet. The outflow of this first "precursor" simulation is then used as inflow of a second computational domain, which models the wind turbines and their wake interactions all the way to the tunnel outlet.

The wind turbines are operated in closed-loop in the CFD simulations, using the same controller implemented in the experiments. The controller receives as inputs power demand P_d, measured power P, measured pitch β and measured rotor speed Ω, and it outputs the pitch command β_{cmd} and torque command T_{cmd}. The implementation is based on a standard look-up table for torque and proportional-integral controller for pitch [12].

The inclusion of the turbine controller in the simulations is important for generating realistic solutions. In fact, the turbulent flows in the experiment and simulation can only be similar in terms of average speed, shear and turbulence intensity, but cannot clearly match instantaneously. Therefore, one can not use in the simulations the blade pitch, rotor speed and azimuthal position measured in the experiments. Even the use of constant values of these quantities would lead to discrepancies, as shown later on in this work.

4. Results and analysis

Iso-vorticity surfaces of the precursor and of the wind turbine cluster simulations are visualized together in Fig. 2. The figure shows the generation of large vortical structures by the spires placed at the tunnel inlet. Such structures break down into a sheared and turbulent flow that becomes the inflow of the downstream turbines.

Figure 3 shows the stream-wise velocity field at a horizontal plane 0.09D above hub height. The images on the top report LiDAR measurements, the ones in the center are the corresponding numerical simulations, while the ones in the bottom part show the difference between measurements and simulations. The rotor planes are drawn using thick black lines. Figures to the left correspond to the case of greedy control, in which all turbines point into the wind. Figures to the right correspond to the case where the two upwind machines have been optimally yawed out of the wind to deflect their wakes and reduce the shading of the downstream turbines. For the LiDAR visualizations, fluctuations in the colors are due to data resolution limits, and to the fact that the number of passes was probably not sufficient to completely eliminate the effects of turbulence and wake meandering. For both the greedy and the optimal yaw cases, the figures show a good qualitative accordance between experiments and simulations. A significant wind farm power increase can be achieved by yaw control in this particular turbine layout and operating conditions. In fact, compared with the baseline greedy case, the optimally-yawed turbine cluster produces 17.6% more power.

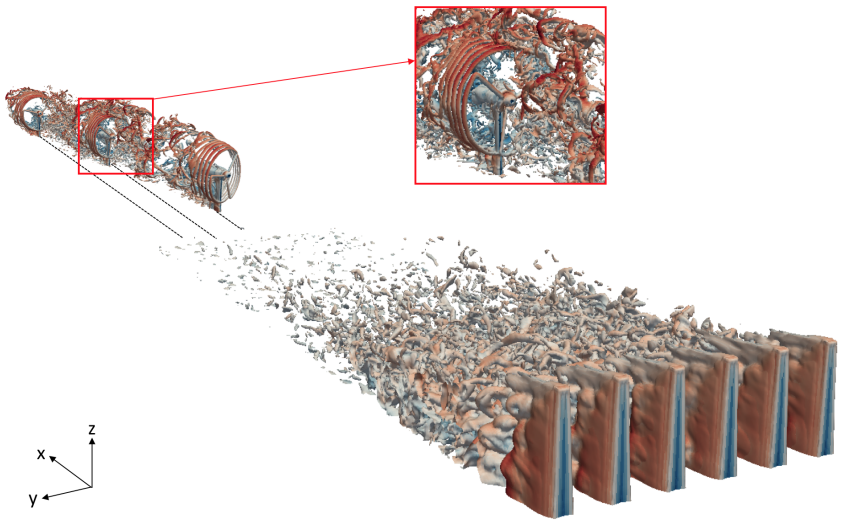

Figure 2: Visualization of iso-vorticity field for the precursor and turbine cluster simulations.

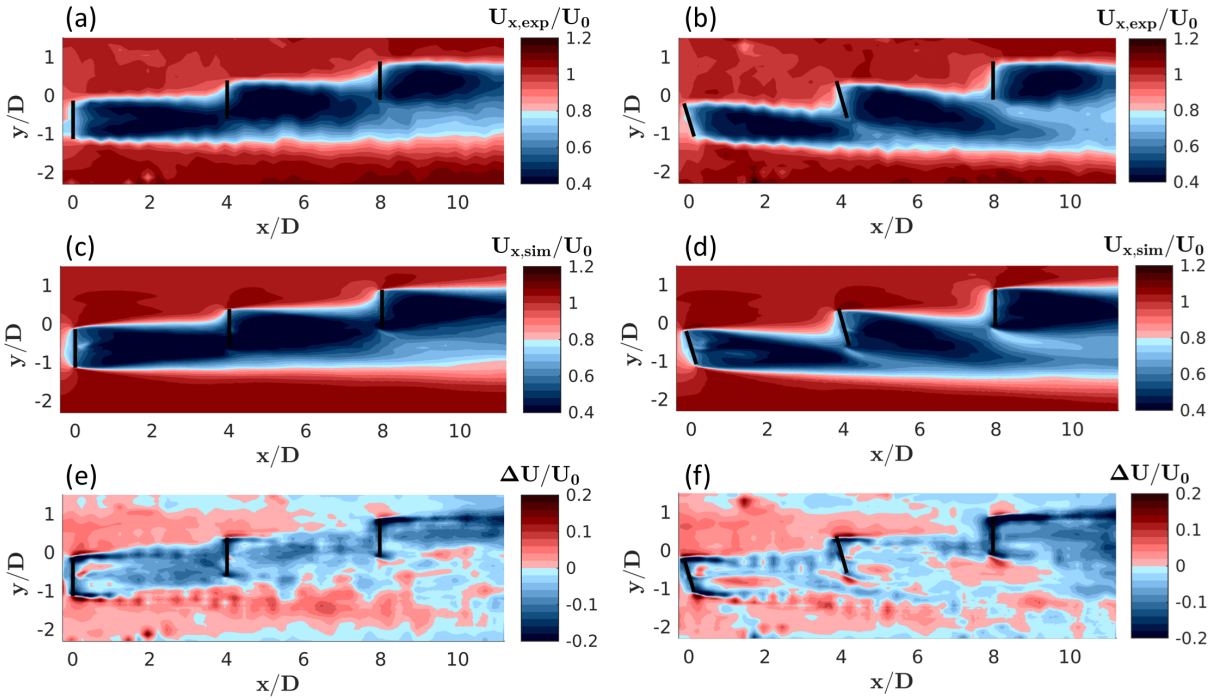

Figure 3: Stream-wise velocity field 0.09D above hub height. (a) Experiment, greedy policy; (b) Experiment, optimal yaw; (c) Simulation, greedy policy; (d) Simulation, optimal yaw; (e) Difference simulation-measurement, greedy policy; (f) Difference simulation-measurement, optimal yaw.

For the optimally-yawed case with turbine controllers in the loop, Fig. 4 shows the time histories of mean power $\bar{P}$ and power standard deviation σ_P defined as:

$$\bar{P}_j = \frac{1}{j}\sum_{i=1}^{j} P_i, \tag{1a}$$

$$\sigma_{P_j} = \sqrt{\frac{1}{j}\sum_{i=1}^{j}(P_i - \bar{P}_j)}, \tag{1b}$$

where P_i is the instantaneous power at the ith step. Goal of these plots is to indicate the necessary time horizon over which one should average in order to compute from instantaneous noisy signals converged mean values and standard deviations for quantities of interest. In both experiments and simulations, the heads of the data streams have been removed to eliminate the effects of initial transients. In the experiments, it takes about 120 sec for the statistics to converge, while it appears that the convergence of the same quantities in simulations takes a much shorter time of about 40 sec. This is because the wind tunnel inflow exhibits moderate low frequency fluctuations due to its closed-loop arrangement. These effects are not reproduced by simulations, which only model the tunnel chamber and not the return flow. Due to their large computational cost, simulations were run for a shorter duration than the experiments. Nonetheless, as shown by the figure, this is still enough to allow for the near converge of the statistics of power. A similar behavior was observed for rotor speed and other quantities of interest.

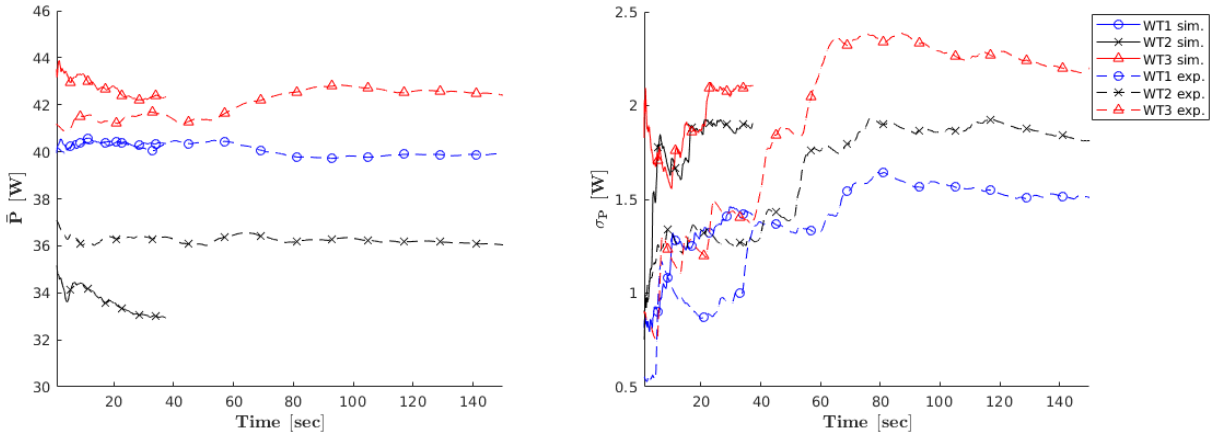

Figure 4: Time histories of mean power $\bar{P}$ and power standard deviation σ_P, indicating that data streams are long enough to compute converged statistics of quantities of interest.

A quantitative comparison between experiments and simulations is obtained by considering wake measurements performed by the scanning LiDARs along sampling lines at various downstream distances, shown in Fig. 5. The sampling lines are orthogonal to the tunnel flow and are located at 0.09D above hub height. The centers of the rotor planes of the three wind turbines are located respectively at 0D, 4D and 8D. Three lines downstream of each machine were measured, resulting in the wake profiles shown in the figure. The top part of the figure reports the greedy case, where all machines point into the wind, while the bottom part of the same figure shows the optimal yaw case.

Although the overall accordance between experiments and simulations is good, there are areas where some small discordancies are indeed present. For the greedy case, the wake deficit of the first wind turbine is overestimated at 2D and 3D, although the wake at 1D is very precisely predicted. This implies a non-exact wake recovery, probably due to an underestimated momentum exchange between free stream and wake. In turn, this is probably due to the blade tip vortices [13], possibly because of an insufficiently refined mesh. An additional reason might be due to inaccuracies in the lifting line formulation at the blade tips, both in terms of angle of attack calculation and distribution of the computed aerodynamic forces back onto the CFD grid. The exact determination of the sources of such discrepancies requires further work. The wake deficit 1D downstream of the second wind turbine is slightly overestimated because of the underestimated inflow wind speed. The wake recovery on the upper side of the figure (i.e., to the left when looking downstream towards the wind turbine cluster) is underestimated. On the other hand, it is interesting to observe that the wake is well predicted in the lower side of the figure because that region interacts with the wake of the upstream wind turbine. Therefore, at 6 and 7D the wake deficit is only underestimated in the left part of the wake. A similar analysis holds for the wake of the third wind turbine.

For the optimally-yawed case, the wakes of the first and second wind turbines are very well predicted, with a very good match between experiments and numerical results. When the turbines are yawed, the inclination of the rotor thrust with respect to the incoming flow induces the generation of two counter rotating vortices in the near wake, that interact with the wake swirling caused by the rotor torque reaction onto the flow. The resulting complex flow pattern contributes to the momentum exchange between free stream and wake, reducing the role of the tip vortices in this process. Because of this, a better match between experiment and simulation is observed in the present case. As expected, since the third wind turbine is not yawed, wake recovery is again slightly underestimated.

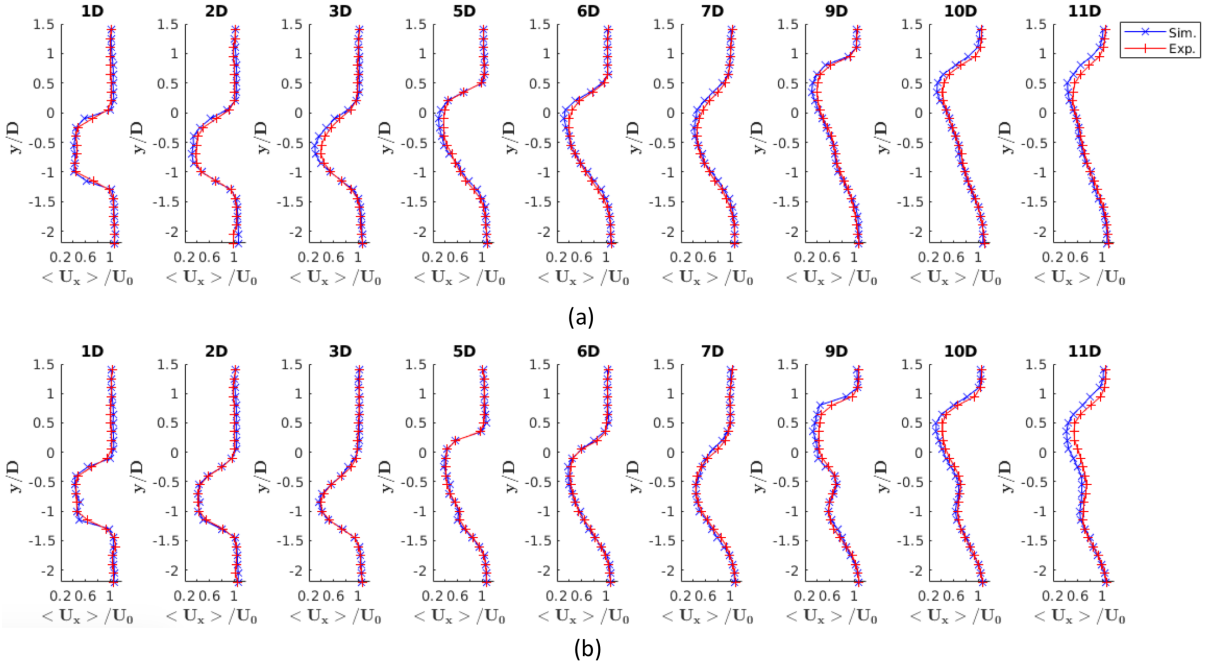

Figure 5: Wake profiles for the greedy (a) and optimally-yawed (b) cases.

Figure 6 shows the time histories of turbine speed and power for the simulations and

experiments in the optimally-yawed case. The figures on the left show the case of the simulation with the controller in the loop; the central plots correspond to the case when the controller is off, and the rotor speed of each machine is constant in time and equal to the average of the experimentally measured one; finally, the plot to the right shows the experimental case. The case with the controller in the loop exhibits a behavior similar to the experimental one, although clearly the instantaneous values cannot match as the two flows are only statistically similar. On the other hand, when the rotors are driven at constant speed, power shows significant and non-physical fluctuations.

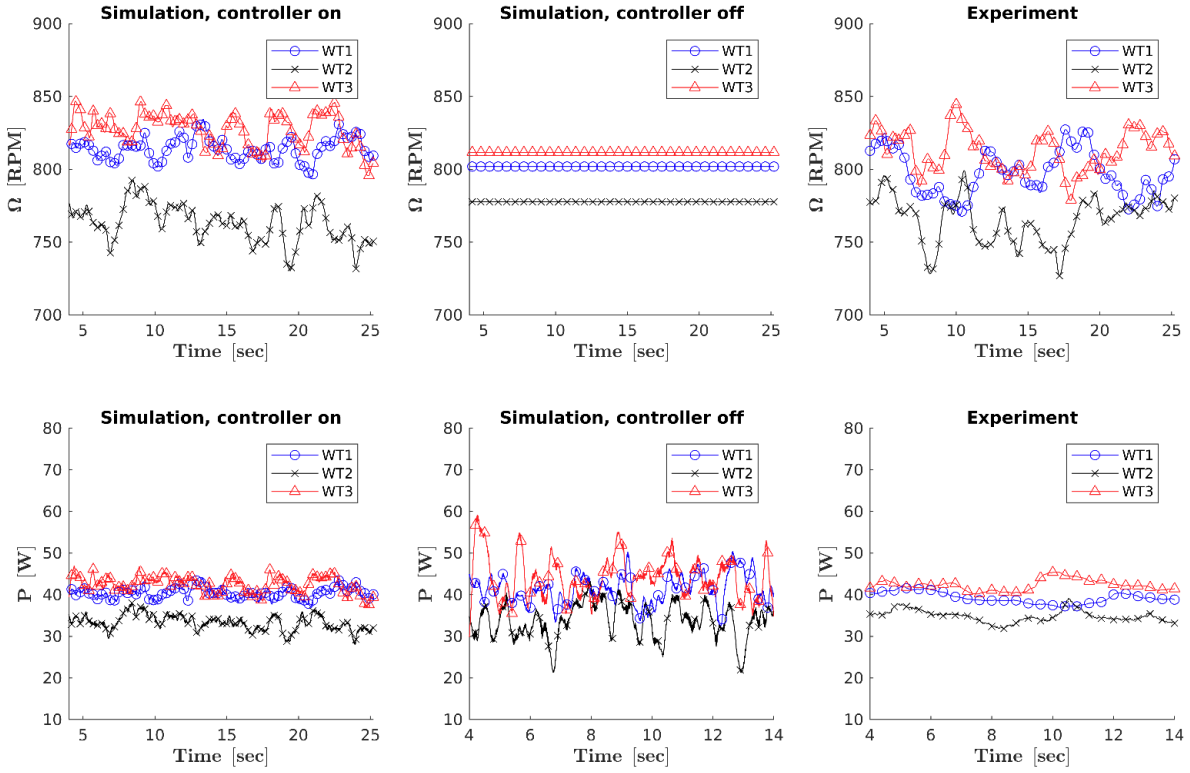

Figure 6: Speed and power time histories for the optimally-yawed case.

For the same three cases (controller in the loop, controller off, and experiment), Table 1 shows the time-averaged means (noted $\overline{(\cdot)}$) and non-dimensional standard deviations σ of rotor speed Ω and power P. Based on the results of Fig. 4, means and standard deviations were computed over 120 sec for the experiments, and over 40 sec for the simulations, which is enough to ensure convergence. The relative error in the average rotor speed for the three turbines is smaller than 2%. Speed variations in the simulations are underestimated, probably because of the assumed constant inflow velocity of the wind tunnel. The average power is predicted quite accurately for both simulations, with and without turbine controllers in the loop. However, as expected, the power standard deviation is much higher when the machines are driven at constant rotor speed.

Table 2 shows the results for the greedy case. The average rotor speed of the second wind turbine is slightly (5%) underestimated because of its underestimated inflow speed. The average speed of the other two wind turbines is very precisely predicted. Speed and power standard deviations for the first wind turbine are underestimated because of the assumption of a constant wind tunnel inflow. The standard deviations of the second and third wind turbines are relatively well predicted because they are more affected by upstream wakes rather than wind tunnel free

stream. For average power, the accordance is in general good, except for the second wind turbine. This situation is visually summarized by the histograms of normalized power shown in Fig. 7 for the various cases and turbines.

Wind turbine	WT1			WT2			WT3		
Case	on	off	exp	on	off	exp	on	off	exp
$\bar{\Omega}$ [RPM]	814	802	802	764	778	778	828	812	812
$\sigma_\Omega/\bar{\Omega}$ [%]	0.9	0	2.1	1.7	0	2.5	1.6	0	2.5
$\bar{P}$ [W]	40.4	41.0	40.5	32.9	33.8	36.4	42.5	43.2	42.0
$\sigma_P/\bar{P}$ [%]	3.2	8.5	4.0	5.5	13.6	5.5	4.7	12.5	4.5

Table 1: Power and speed comparisons for the optimally-yawed case.

Wind turbine	WT1			WT2			WT3		
Case	on	off	exp	on	off	exp	on	off	exp
$\bar{\Omega}$ [RPM]	840	830	830	672	710	710	734	736	736
$\sigma_\Omega/\bar{\Omega}$ [%]	0.5	0	2.0	1.7	0	2.7	1.9	0	3.0
$\bar{P}$ [W]	44.5	45.7	44.3	22.8	21.5	26.5	29.5	29.1	30.3
$\sigma_P/\bar{P}$ [%]	1.8	9.0	3.1	6.6	28.8	7.1	7.1	26.8	6.9

Table 2: Power and speed comparisons for the greedy case.

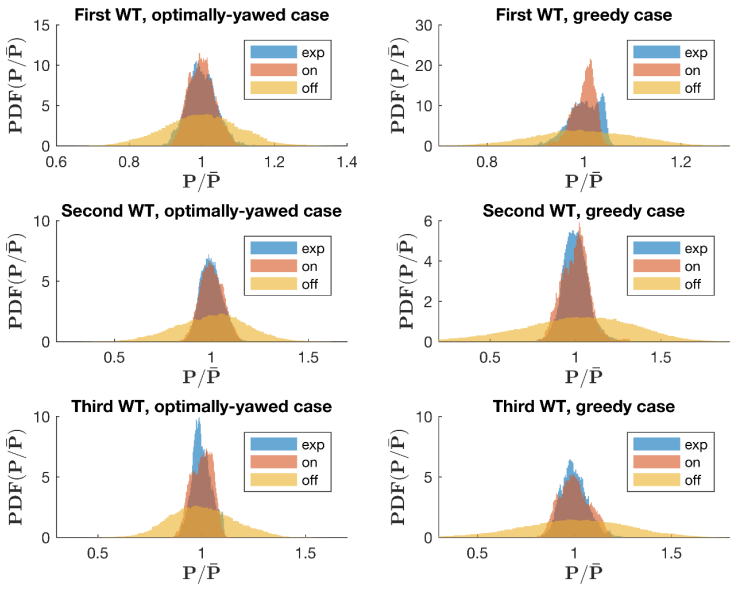

Figure 7: Wind turbine power histogram for simulations and experiments.

5. Effects of wake shading on wake deflection

An interesting phenomenon can be observed in Fig. 3 for both the experimental and the simulation results. In fact, for the optimally-yawed case, it appears that the wake of the second wind turbine is more deflected than the wake of first machine, although the yaw angle of the second (16 deg) is smaller than the one of the first (20 deg).

This phenomenon is caused by the changed inflow conditions for the second shaded wind turbine, caused by the presence of the wake shed by the upstream machine. To better illustrate this phenomenon, a simulation was run with one single wind turbine operating exactly in the same conditions of the first upstream machine (the effects of the two downstream machines on the inflow of the first one being negligible). For this single turbine simulation, Fig. 8 shows the stream-wise and lateral velocity components, respectively to the left and to the right of the picture. Although the second and third turbines are not present in this simulation, their rotor planes are still plotted in dotted lines to indicate their location within the cluster.

When looking at the stream-wise velocity component, it appears that the wake of the first turbine has only a modest overlap with the rotor disk of the second machine. On the other hand, the analysis of the lateral velocity component reveals a very different situation. In fact, the rotor disk of the second turbine is immersed in a region of significant sidewash caused by the wake of the upstream machine. This sidewash component, combined with the incoming free stream, generates a tilting of the local wind vector of about 3.6 deg. Therefore, while the misalignment angle of the second wind turbine with the free stream is nominally equal to 16 deg, its *actual* misalignment with the *local* wind vector is about 19.6 deg. This value is quite close to the misalignment angle of the first wind turbine, which is equal to 20 deg.

Therefore, the additional deflection of the wake observed for the second machine can be justified based on the sidewash velocity of the impinging wake. Indeed, this additional lateral wind component causes two effects: a) it tilts the local wind vector, which has the effect of modifying the actual misalignment angle of the turbine, and b) it carries the wake shed by the second machine sideways, further incrementing its deflection. In present engineering wake models, little attention has been paid so far to the changed ambient velocity outside of the central wake region. Indeed, according to the authors' knowledge, published engineering wake models only represent what happens inside the wake, but not outside of it. However, the current results seem to indicate that the induced lateral velocity outside of a deflected wake should be taken into due account for an accurate prediction of the wake path of shaded wind turbines.

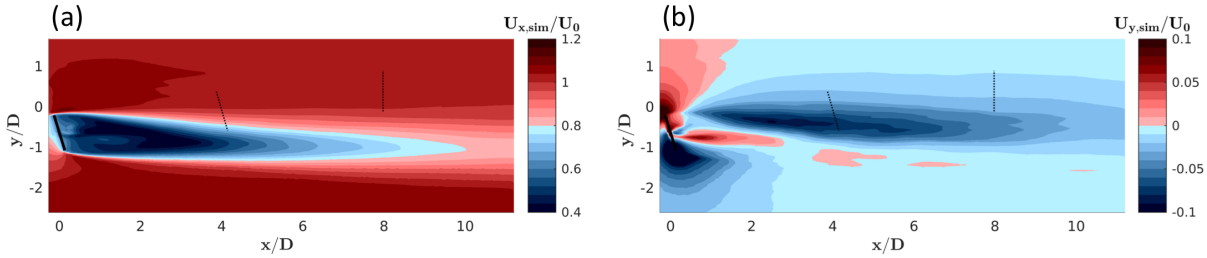

Figure 8: Wake of a single yawed wind turbine: (a) stream-wise velocity (b) lateral velocity. Dashed lines indicate position and orientation of the downstream machines in the cluster. Negative values of the lateral velocity indicate a velocity directed downwards in the picture.

6. Conclusion

In this paper, numerical simulations were performed for scaled waked wind turbines at given fixed yaw settings. The flow within the scaled wind turbine cluster and the operational response

of the machines show a good match between simulations and measurements. In particular, the simulation model appears to be capable of predicting with good accuracy the wake behavior and power output of the various wind turbines. The tool appears to be mature enough to consider the dynamic case where yaw angles change in time, which will be the subject of future work.

Besides the validation of the numerical method, this paper also exploits the numerical model to interpret and explain wake interference effects. Specifically, it appears that the sidewash caused around a deflected wake has non-negligible effects on the path of downstream wakes, effects that are currently not accounted for in engineering wake models.

7. Acknowledgements

This work has been supported by the CL-WINDCON project, which receives funding from the European Union Horizon 2020 research and innovation program under grant agreement No. 727477. The authors also express their appreciation to the Leibniz Supercomputing Centre (LRZ) for providing access and computing time on the SuperMUC Petascale System.

References

[1] Churchfield M J, Fleming P, Bulder B, et al. 2015 *Wind Turbine Wake-Redirection Control at the Fishermen's Atlantic City Windfarm* Preprint OTC-25644-MS
[2] Campagnolo F, et al. 2016 Wind tunnel testing of a closed-loop wake deflection controller for wind farm power maximization *J. Phys. Conf. Seri.* **753**(3) 032006
[3] Dooren M F, Campagnolo F, Sjholm M, Angelou N, Mikkelsen T and Khn M, 2017 Demonstration and uncertainty analysis of synchronised scanning LiDAR measurements of 2-D velocity fields in a boundary-layer wind tunnel *Wind Energy Science* **2**(1) 329
[4] Fleming, Paul A, et al. 2014 Evaluating techniques for redirecting turbine wakes using SOWFA *Renewable Energy* **70** 211–218
[5] Guntur S, Jonkman J, et al. 2016 FAST v8 verification and validation for a MW-scale Wind turbine with aeroelastically tailored blades *Wind Energy Symp.* (San Diego, USA) p. 1008
[6] Peskin, Charles S. 2002 The immersed boundary method *Acta numerica* **11** 479–517.
[7] Bottasso C L, Stefano C, et al. 2014 Calibration of wind turbine lifting line models from rotor loads *J. Wind Engineering and Industrial Aerodynamics* **124** 29-45.
[8] Wang J, Mclean D, et al. 2017 Large-eddy simulation of waked turbines in a scaled wind farm facility *J. Phys. Conf. Seri.* **854**(1) 012047
[9] Wang J, Bottasso C L, et al. 2016 Wake redirection: comparison of analytical, numerical and experimental models *J. Physics: Conf. Seri.* **753**(3) 032064
[10] Wang, J., et al. 2017 *Numerical and experimental study of wake redirection techniques in a boundary layer wind tunnel* J. of Phys. Conf. Seri. **854**(1) 012048
[11] Foti D, Yang X, Campagnolo F, et al. Wake meandering of a model wind turbine operating in two different regimes *Physical Review Fluids* under review
[12] Bottasso C L, Campagnolo F, et al. 2014 Wind tunnel testing of scaled wind turbine models: beyond aerodynamics *J. Wind Engineering and Industrial Aerodynamics* **127** 11–28
[13] Wang J, Chengyu W, Campagnolo F and Bottasso C L 2018 A large-eddy simulation approach for wind turbine wakes and its verification with wind tunnel measurements *Wind Energy Science* under review